Induced Fit Activity-Based Sensing: A Mechanistic Study of Pyrophosphate Detection with a "Flexible" Fe-Salen Complex

Prerna Yadav[a], Olivier Blacque[a], Andreas Roodt [b*] and Felix Zelder[a*]

[a]Department of Chemistry, University of Zurich, Winterthurerstrasse 190, CH-8057 Zurich, Switzerland. Fax: +41 44 635 6803; E-mail: felix.zelder@chem.uzh.ch, www.felix-zelder.net.

[b]Department of Chemistry, University of the Free State, PO Box 339, Bloemfontein 9300, South Africa. www.ufs.ac.za/natagri/departments-and-divisions/chemistry-home/general/staff Tel: 051 4012547; E-mail: RoodtA@ufs.ac.za

Contents

S1. Calculations and Models

S1.1 Basic Equations/ Models

All calculations were done by Least-Squares (L.S.) fitting with *ORIGIN* or *Micromath SCIENTIST* program suites, using of the data points to appropriate functions. The following basic equations were used, wherein appropriate independent and dependent variables, and parameters were identified, fitted to appropriate relevant data sets:

First-order fitting of Absorbance/Fluorescence vs time data:

$$A_{obs} = A_\infty - (A_\infty - A_0)e^{(-k_{obs.} t)}\} \qquad \dots\text{(i)}$$

At pH values of around 5 and higher the principal pyrophosphate species are, $H_2P_2O_7^{2-}$ $HP_2O_7^{3-}$ and $P_2O_7^{4-}$ thus

$$[PPi]_{tot} = [H_2P_2O_7^{2-}] + [HP_2O_7^{3-}] + [P_2O_7^{4-}] \qquad \dots\text{(ii)}$$

By incorporating the definitions of the Bronsted acid dissociation constants K_{a2}, K_{a3} and K_{a4} for the pyrophosphate, reorganising, and introducing Equation (ii) therein, Equation (iii) is obtained in terms of the total $[PPi]_{tot}$ for the concentration of the identified primary reactive pyrophosphate species, $HP_2O_7^{3-}$:

$$[HP_2O_7^{3-}] = [PPi]_{tot}(K_{a3}/[H^+])/\{1 + (K_{a3}/[H^+]) + (K_{a3}K_{a4}/[H^+]^2)\} \qquad \dots\text{(iii)}$$

Assuming fast multi-step pre-equilibria (Reactions II and III), with a rate determining final step (Reaction IV), as illustrated in Equation (iv) gives the expression for the *pseudo* first-order rate constant k_{obs}, as shown in Eq. (v), following the incorporation of the pK_a values of both the PPi and the Fe-salen (**1-OH₂**) complex:

$$1\text{-OH}_2 + PPi \underset{\text{(II-III)}}{\overset{K_{eq}}{\rightleftharpoons}} [3] \xrightarrow[\text{(IV)}]{k_{PPi}} 5 \qquad \dots\text{(iv)}$$

$$k_{obs} = k_{PPi}K_{eq}[PPi]/(1 + K_{eq}[PPi]) \qquad \dots\text{(v)}$$

$$k_{obs} = \underline{(k_{PPi}K_{eq}\{[PPi]_{tot}(K_{a3}/[H^+])/\{1+(K_{a3}/[H^+])+(K_{a3}K_{a4}/[H^+]^2)\}\})}$$
$$\{1+(K_a/[H^+])+(K_{eq}\{[PPi]_{tot}(K_{a3}/[H^+])/\{1+(K_{a3}/[H^+])+(K_{a3}K_{a4}/[H^+]^2)\}\})\} \quad \dots\text{(vi)}$$

From these fits, values of k_{PPi} and K_{eq} were obtained, as listed.

Equation (vi) also defines the pH dependence of the *pseudo* first-order rate constant as a function of the species distribution of the PPi and **1-OH$_2$**. In this case, all known parameters were fixed, allowing the pH to vary.

Temperature studies were finally completed. In these, a model consisting of a combination of Equation (vi) and the Eyring equation, Equation (vii) was done, thus yielding the activation parameters ($\Delta S^{\neq}$ and $\Delta H^{\neq}$) directly from 26 observations (Table S2). This model required two independent variables (T, [PPi]$_{tot}$), with k_{obs} the dependent variable.

$$k = (k_B T/h) \cdot e^{(\Delta S^{\neq}/R)} \cdot e^{(-\Delta H^{\neq}/RT)} \qquad \text{...(vii)}$$

k_B = Boltzmann constant (1.380649×10^{-23} J K^{-1})

T = Temperature (in K)

h = Planck's constant ($6.62607015 \times 10^{-34}$ J s)

k = Reaction rate constant (in s^{-1})

$\Delta S^{\neq}$ = Entropy of activation (in J K^{-1} mol^{-1})

$\Delta H^{\neq}$ = Enthalpy of activation (in kJ mol^{-1})

S1.2. Examples of L.S. Fits to Determine the *Pseudo* First-Order Rate Constants
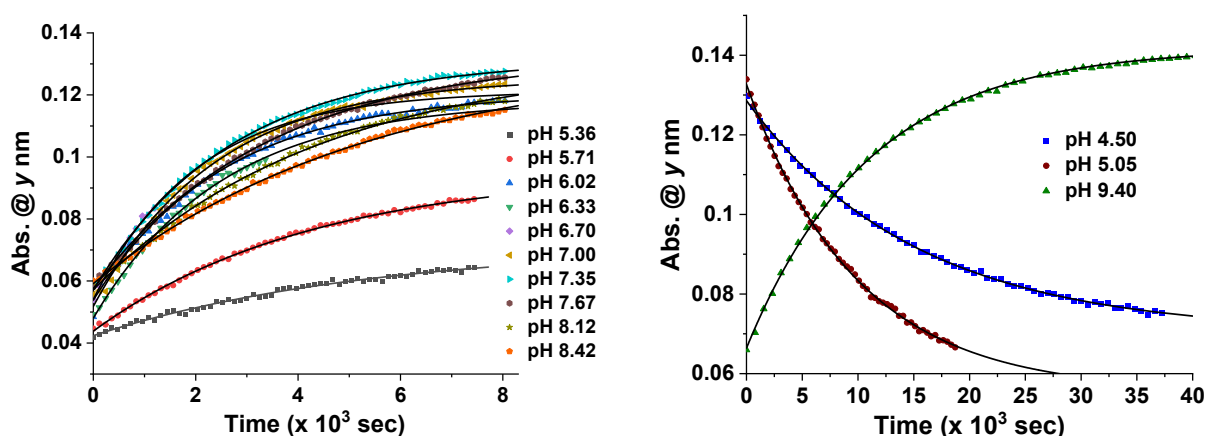
Figure S1. *Left:* Changes in absorbance of **1-OH$_2$** (16 µM) in presence of PPi (10 equiv; 0.16 mM) at *y* nm (*y* = between 375 to 385 nm) with time at 10 different pH from 5.36 to 8.42 at 25 °C and their respective individual *pseudo* first-order kinetic fits. *Right:* Changes in absorbance of **1-OH$_2$** (16 µM) in presence of PPi (10 equiv; 0.16 mM) at *y* nm (*y* = 324 nm (pH 4.50), 322 nm (pH 5.05), 378 nm (pH 9.40)) with time at 3 different pH[*] (4.50, 5.05 and 9.40) at 25 °C along with their respective individual *pseudo* first-order kinetic fits. [Lines indicate L.S. fits]

[*]First-order kinetic traces are shown separately for two acidic pH and one basic pH. At acidic pH, considerable changes in absorbance occur at lower wavelengths in comparison to that of other tested pH values.

Table S1. List of observed *pseudo* first-order rate constants for reaction of **1-OH$_2$** (16 µM) and PPi (10 equiv; 0.16 mM) at 13 different pH values at 25 °C.

pH	k_{obs} (sec^{-1} × 10^{-3})
4.50	0.066 ± 0.001
5.05	0.100 ± 0.002
5.36	0.19 ± 0.01
5.71	0.234 ± 0.004
6.02	0.370 ± 0.008
6.33	0.40 ± 0.02
6.70	0.40 ± 0.02
7.00	0.420 ± 0.006
7.35	0.369 ± 0.004
7.67	0.293 ± 0.003
8.12	0.225 ± 0.005
8.42	0.180 ± 0.004
9.40	0.090 ± 0.001

S2. Mechanism and Rate Law

Derivation of Rate Law: Disassembly of the Fe^{III}-complex (1-OH$_2$) by Pyrophosphate (PPi)

The total Rate law for the Disassembly of **1-OH$_2$** is derived based on Scheme 1:
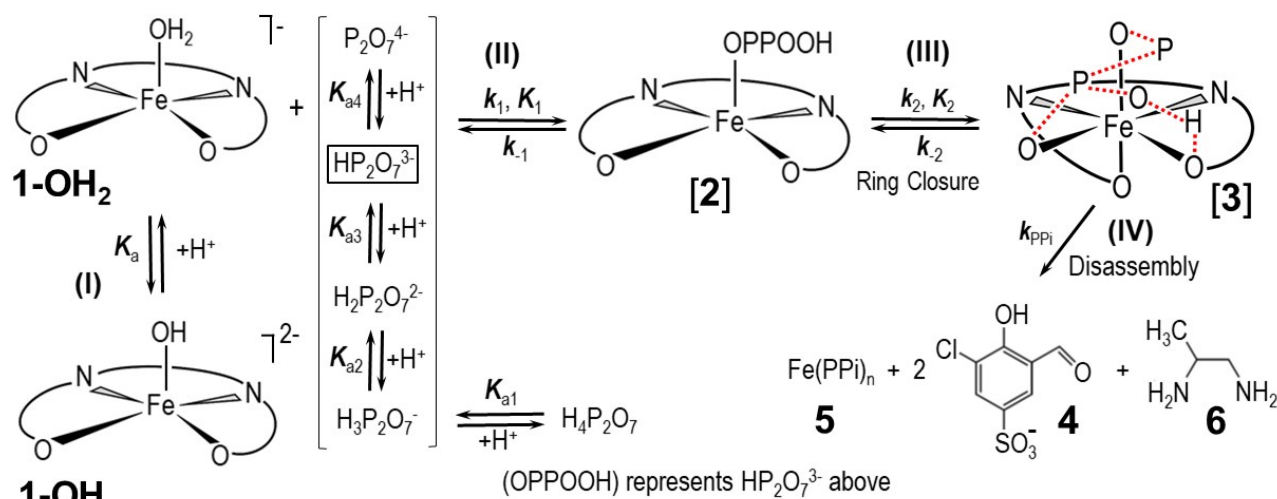
Scheme 1. Simplified reaction scheme for the disassembly as studied kinetically, with **1-OH$_2$** and **1-OH** {interrelated by the acid dissociation constant K_a, and with $[1]_{tot} = [1\text{-}OH_2] + [1\text{-}OH]$}; **[2]** and **[3]** are assumed reactive intermediate species, **5** = final Fe-PPi species; **4** = 3-chloro-5-sulfosalicylaldehyde. Moreover $[PPi]_{tot}$ = total pyrophosphate concentration, of which the parent tetra-acid exhibits four pK_a values, denoted by K_{a1}, K_{a2}, K_{a3} and K_{a4}. Note that all charges are omitted for simplicity.

1. Consider the species numbering as follows: **1-OH$_2$**, **1-OH**, {with $[Fe]_{tot} = [1]_{tot} = [1\text{-}OH_2] + [1\text{-}OH]$}; **[2]** (with PPi = mono-coordinated, **[3]** (PPi = bidentate coordinated with possible hydrogen bonding), **4** = 3-chloro-5-sulfosalicylaldehyde; **5** = Fe(PPi)$_n$. ; the final Fe-complex after disassembly. Charges are omitted. Moreover $[\mathbf{PPi}]_{tot}$ = total pyrophosphate concentration, of which the parent tetra-acid exhibits four pK_a values, denoted by K_{a1}, K_{a2}, K_{a3} and K_{a4}.[S1]

2. The above reaction scheme was concluded based on the following systematic experiments:

(a) **1-OH$_2$** acts as a monoprotic acid (with the formation of the hydroxido species) and exhibits a pK_a value, denoted by pK_a of 6.90, as determined from a potentiometric titration, see Reaction (I).[S2]

(b) From a pH variation at fixed $[PPi]_{tot}$ and $[\mathbf{1}]_{tot}$ a significant rate increase was observed where the monoprotonated tri-anion, $HP_2O_7^{3-}$, is the principal pyrophosphate species in solution. However, the maximum rate was reached where the product of the populations of $[\mathbf{1}$-$\mathbf{OH_2}][HP_2O_7^{3-}]$ was a maximum (see Figure 4).

(c) Upon variation of $[PPi]_{tot}$ at this pH, a rate-limiting dependence on $[PPi]_{tot}$, as manifested in a plateau reached, was observed, indicating a potential rapid pre-equilibrium reaction (in the above mentioned scheme indicated by the combination of Reaction (II) and (III)), denoted by $K_{eq} = K_1 K_2$, and a consecutive rate limiting first-order formation of $\mathbf{5}$ (holding also for the formation of $\mathbf{4}$), denoted by k_{PPi}.

(d) The formation of species $\mathbf{5}$, assuming to be an Fe^{III}-pyrophosphate species, is generated in a rate-determining step as defined in Reaction IV and was studied by an extended UV/Vis kinetic study.

(e) The generation of fluorescence (studied by a fluorescence kinetic study) coincides exactly with Reaction IV, following an "induction period" of a few minutes, assumed to be representing the formation of $\mathbf{4}$.

(f) The "induction period" observed from the above indicates potentially two relatively quick pre-equilibria, denoted by Reactions (II) and (III) in the above scheme, in agreement with (c) above.

(g) Upon analysis of the UV/Vis spectra at the isosbestic point (at $\lambda = 385nm$) the pre-reactions attributed to the "induction period" are clearly observed, and again agrees with the fluorescence data. It is however noted that the Absorbance/Fluorescence contributions of these assumed pre-equilibria to the total Abs/F.I. are small (see Figures 3 and 6, and Section S5).

(h) Attempted study of Reaction (II) using monodentate entering nucleophile F^-, only resulted in slower reactions, indicating non-favourable reactions, and in agreement with potential *decomposition* of the parent complex.

3. From the above, the Rate Law describing the experimental observations is derived, as discussed below.

The formation of species $\mathbf{5}$ is given by Equation 1: $d[\mathbf{5}]/dt = k_{PPi}[\mathbf{3}]$　　　　　…(1)

There is, from the pH variation experiments, some indication of a slow, concurrent reaction parallel to k_{PPi} as the principal one, defined by a rate constant k_{22}. If this is the case, an additional step, not indicated in Scheme 1, may be considered (typically, a slow background hydrolysis, see Discussion in manuscript). This is for completeness indicated in Equation 15, but not analysed further within this study.

Assuming that only the $HP_2O_7^{3-}$ reacts with the aqua species **1-OH₂**, the pre-equilibria in Reaction (II) and (III) can be written by Equation 2 and 3:

$$K_1 = [\mathbf{2}]/([\mathbf{1\text{-}OH_2}][HP_2O_7^{3-}]) \qquad \dots(2)$$

$$K_2 = [\mathbf{3}]/[\mathbf{2}] \qquad \dots(3)$$

The overarching equilibrium from **1-OH₂** *via* **2** to **3** is then given by Equation 4:

$$K_1K_2 = K_{eq} = [\mathbf{3}]/([\mathbf{1\text{-}OH_2}][HP_2O_7^{3-}]) \qquad \dots(4)$$

When defined as a monoprotic acid, the acid dissociation constant for **1-OH₂** is given by Equation 5:

$$K_a = ([\mathbf{1\text{-}OH}][H^+])/[\mathbf{1\text{-}OH_2}] \qquad \dots(5)$$

Moreover, the total reactant Fe^{III} in solution is given by Equation 6, which upon introducing Equation 5, yields Equation 7:

$$[\mathbf{1}]_{tot} = [\mathbf{1\text{-}OH}] + [\mathbf{1\text{-}OH_2}] \qquad \dots(6)$$

Thus,

$$[\mathbf{1\text{-}OH_2}] = [\mathbf{1}]_{tot}/(K_a/[H^+]) \qquad \dots(7)$$

At pH values of around 5 and higher the principal pyrophosphate species are, $H_2P_2O_7^{2-}$ $HP_2O_7^{3-}$ and $P_2O_7^{4-}$ thus

$$[PPi]_{tot} = [H_2P_2O_7^{2-}] + [HP_2O_7^{3-}] + [P_2O_7^{4-}] \qquad \dots(8)$$

Based on the definitions of K_{a2}, K_{a3} and K_{a4}, reorganising, and introducing in Equation 8, Equation 9 is obtained for the assumed primary reactive pyrophosphate species, $HP_2O_7^{3-}$:

$$[HP_2O_7^{3-}] = [PPi]_{tot}(K_{a3}/[H^+])/\{1 + (K_{a3}/[H^+]) + (K_{a3}K_{a4}/[H^+]^2)\} \qquad \dots(9)$$

Before Reaction (IV) commences, the total amount of Fe^{III} {$[\mathbf{1}]_{tot}$; i.e. the amount Fe^{III} started with} is given by uncoordinated Fe^{III} {$[FeO]_{tot}$} and coordinated Fe^{III} {$[\mathbf{3}]$} as shown by Equation 10:

$$[\mathbf{1}]_{tot} = [FeO]_{tot} + [\mathbf{3}] \qquad \qquad ...(10)$$

Introducing Equation 7 into Equation 4 yields Equation 11:

$$K_{eq} = [\mathbf{3}]/\{[FeO]_{tot}/(1 + K_a/[H^+])[HP_2O_7^{3-}]\} \qquad ...(11)$$

Reorganising Equation 11 yields Equation 12:

$$[FeO]_{tot} = [\mathbf{3}](1 + K_a/[H^+])/(K_{eq}[HP_2O_7^{3-}]) \qquad ...(12)$$

Introducing Equation 12 into Equation 10 yields Equation 13 after re-organising, which can be further manipulated to give Equation 14:

$$[\mathbf{1}]_{tot} = [\mathbf{3}](1 + K_a/[H^+])/(K_{eq}[HP_2O_7^{3-}]) + [\mathbf{3}] \qquad ...(13)$$

Thus

$$[\mathbf{3}] = \{[\mathbf{1}]_{tot}/\ \{(1 + K_a/[H^+])/(K_{eq}[\cancel{HP_2O_7^{3-}}]) + 1\}\} \text{ x } (K_{eq}[HP_2O_7^{3-}]/\ K_{eq}[\cancel{HP_2O_7^{3-}}])$$

or

$$[\mathbf{3}] = ([\mathbf{1}]_{tot}K_{eq}[HP_2O_7^{3-}])/\{1\ + (K_a/[H^+]) + (K_{eq}[HP_2O_7^{3-}])\} \qquad ...(14)$$

By introducing (i) Equation 9 in Equation 14, and (ii) the resultant into Equation 1, and (iii) assuming $[PPi]_{tot} \gg [\mathbf{1}]_{tot}$ (*pseudo* first-order conditions) the total expression for the *pseudo* first-order rate constant ($\boldsymbol{k}_{obs}$) from this Rate Law for the formation of the final product(s) **4**, **5** is obtained as given in Equation 15:

$$\boldsymbol{k}_{obs} = k_{PPi}[\mathbf{3}]$$
$$= \frac{(k_{PPi}K_{eq}\{[PPi]_{tot}(K_{a3}/[H^+])/\{1+(K_{a3}/[H^+])+(K_{a3}K_{a4}/[H^+]^2)\}\})}{1+(K_a/[H^+])+(K_{eq}\{[PPi]_{tot}(K_{a3}/[H^+])/\{1+(K_{a3}/[H^+])+(K_{a3}K_{a4}/[H^+]^2)\}\})\}} + k_{22}\,...(15)$$

Equation 15 describes the total pH dependence of the reaction as studied, and was utilised in the L.S. fits of the (i) pH variation, (ii) the evaluation of the effect of total pyrophosphate and the (iii) temperature study (see Figures 4, 5 and 6, respectively).

S3.   Least-Squares Fits of Absorbance (Fluorescence) vs Time data
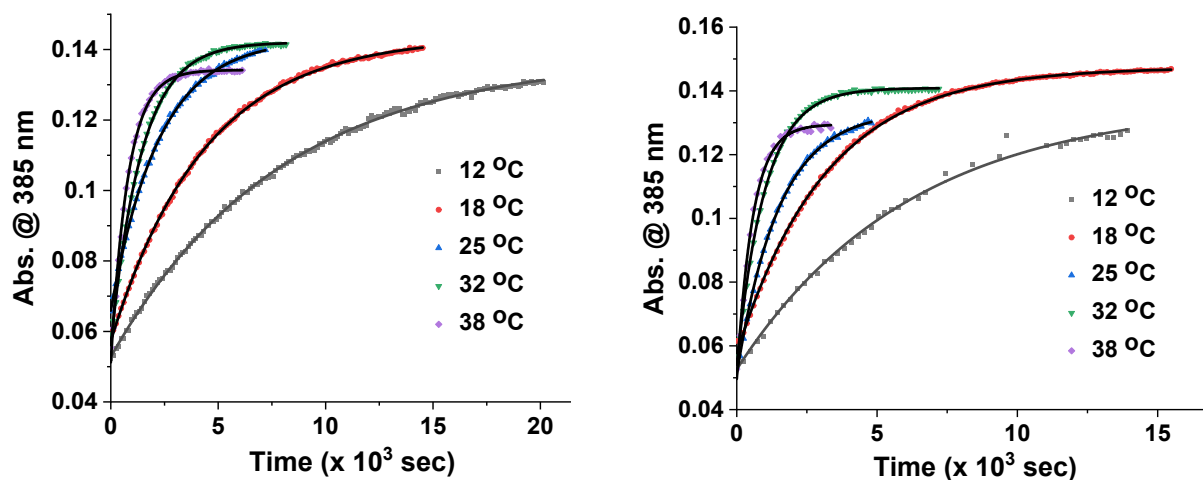
Figure S2. *Left*: Changes in absorbance at 385 nm of **1-OH₂** (16 μM) in presence of PPi (10 equiv; 0.16 mM) with time at 5 different temperatures at pH 7.35 ([Tris buffer] = 10 mM) and their individual *pseudo* first-order kinetic fits. *Right:* Changes in absorbance at 385 nm of **1-OH₂** (16 μM) in presence of PPi (15 equiv; 0.24 mM) with time at 5 different temperatures at pH 7.35 ([Tris buffer] = 10 mM) and their individual *pseudo* first-order kinetic fits. [Lines indicate L.S. fits]
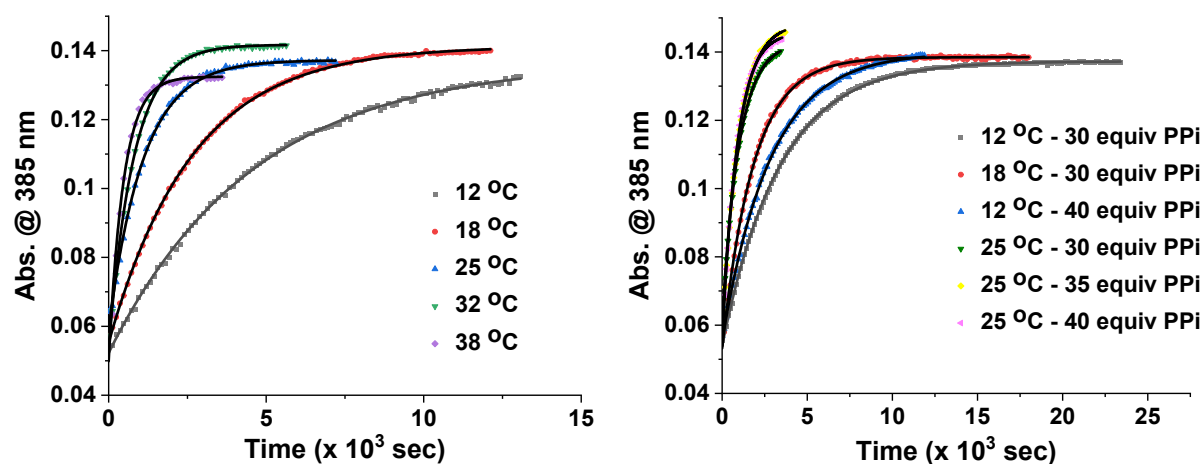
Figure S3. *Left*: Changes in absorbance at 385 nm of **1-OH₂** (16 μM) in presence of PPi (20 equiv; 0.32 mM) with time at 5 different temperatures at pH 7.35 ([Tris buffer] = 10 mM) and their individual *pseudo* first-order kinetic fits. *Right:* Changes in absorbance at 385 nm of **1-OH₂** (16 μM) in presence of PPi (30 equiv; 0.48 mM, 35 equiv; 0.56 mM, 40 equiv; 0.64 mM) with time at 3 different temperatures at pH 7.35 ([Tris buffer] = 10 mM) and their individual *pseudo* first-order kinetic fits. [Lines indicate L.S. fits]
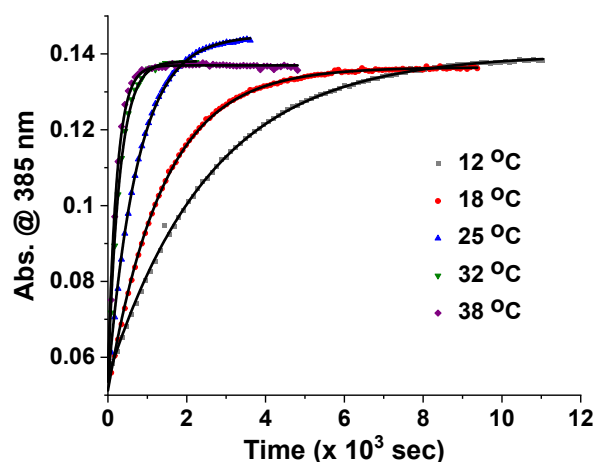
Figure S4. Changes in absorbance at 385 nm of **1-OH₂** (16 µM) in presence of PPi (50 equiv; 0.80 mM) with time at 5 different temperatures at pH 7.35 ([Tris buffer] = 10 mM) and their individual *pseudo* first-order kinetic fits. [Lines indicate L.S. fits]

Table S2. List of k_{obs} values at different temperatures for different conc. of PPi at pH 7.35

[PPi]$_{tot}$ (M × 10⁻³)	12 °C	18 °C	25 °C	32 °C	38 °C
			k_{obs} (sec⁻¹ × 10⁻³)		
0.16	0.127 ± 0.001	0.229 ± 0.001	0.444 ± 0.004	0.704 ± 0.005	1.25 ± 0.02
0.24	0.163 ± 0.006	0.314 ± 0.001	0.687 ± 0.008	0.992 ± 0.009	1.76 ± 0.04
0.32	0.217 ± 0.002	0.376 ± 0.002	0.952 ± 0.007	1.240 ± 0.014	2.11 ± 0.06
0.48	0.295 ± 0.001	0.540 ± 0.002	1.025 ± 0.008	-	-
0.56	-	-	1.091 ± 0.008	-	-
0.64	0.351 ± 0.002	-	1.22 ± 0.01	-	-
0.80	0.383 ± 0.003	0.714 ± 0.004	1.38 ± 0.01	2.430 ± 0.002	4.12 ± 0.03

([Tris buffer] = 10 mM). *

(a)

(b)
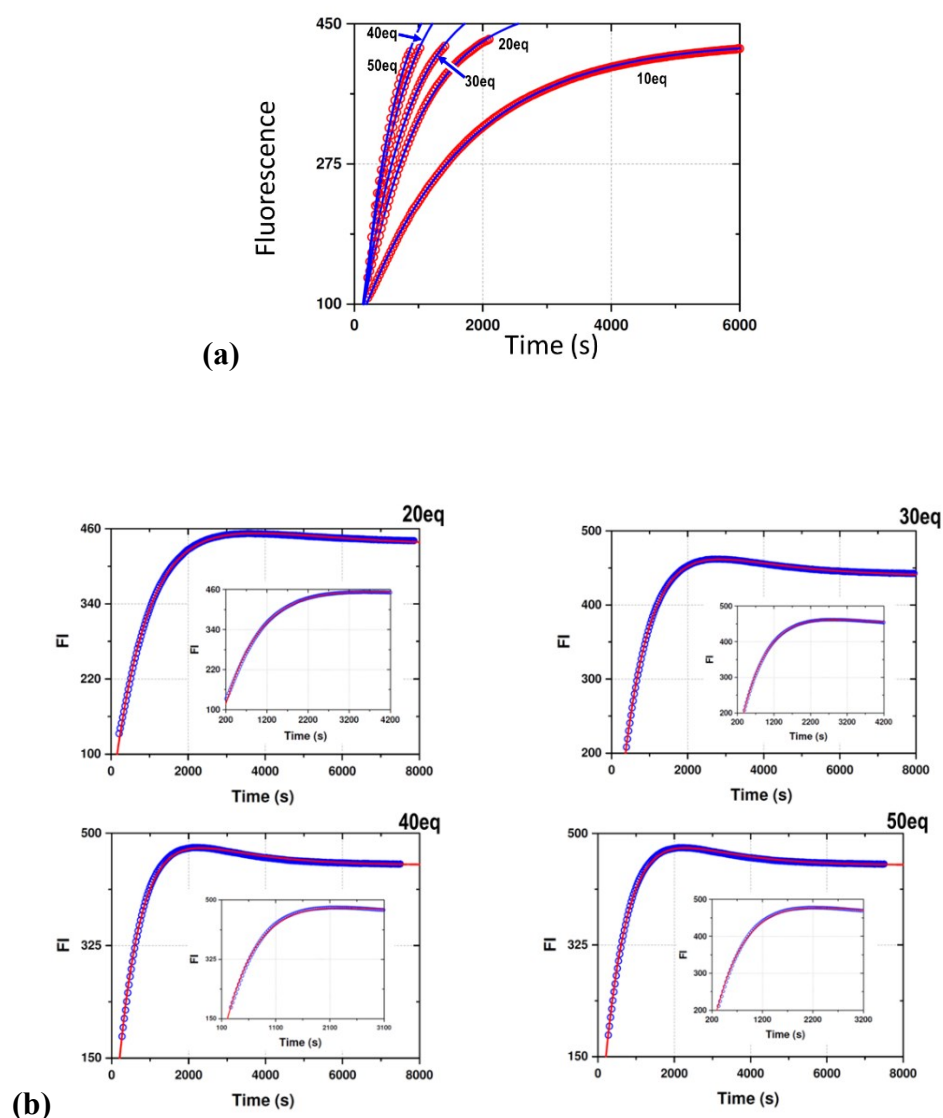
Figure S5. Changes in fluorescence intensity at 500 nm (λ_{ex} = 385 nm) of **1-OH$_2$** (16 µM) in presence of 5 different conc. of PPi with time at 28 °C at pH 7.35 ([Tris buffer] = 10 mM) and their individual kinetic fits. [Lines indicate L.S. fits]. (a) First part of reaction fitted to a single exponential [Eq. (i) above]; (b) total reaction [except 10 eq PPi, which showed no 2nd reaction, see (a)] fitted to the two-exponential function describing two consecutive reactions : $A_{obs}=A_{B\infty}-(A_{A\infty}-A_{A0})Exp(-k_{ab}.t)-(A_{B\infty}-A_{A\infty})Exp(-k_{bc}.t)$; with A=Abs or FI.

Table S3. List of k_{obs} values from fluorescence kinetic traces at different conc. of PPi at 28 °C at pH 7.35 ([Tris buffer] = 10 mM). [Fits in Figure S5]

[PPi] (M × 10⁻³)	k_{obs} (sec⁻¹ × 10⁻³)	
	Single exponential fit [a]	Two exponential fit [b]
0.16	0.610 ± 0.001	0.610 ± 0.003
0.32	1.111 ± 0.008	1.100 ± 0.005
0.48	1.30 ± 0.02	1.280 ± 0.006
0.64	1.52 ± 0.04	1.510 ± 0.006
0.80	1.80 ± 0.07	1.70 ± 0.01

[a] Figure S5(a) [b] Figure S5(b); $A_{obs} = A_{B\infty} - (A_{A\infty}-A_{A0})\mathrm{Exp}(-k_{ab}.t) - (A_{B\infty}-A_{A\infty})\mathrm{Exp}(-k_{bc}.t)$

S4.   Global Fit of Kinetic Data
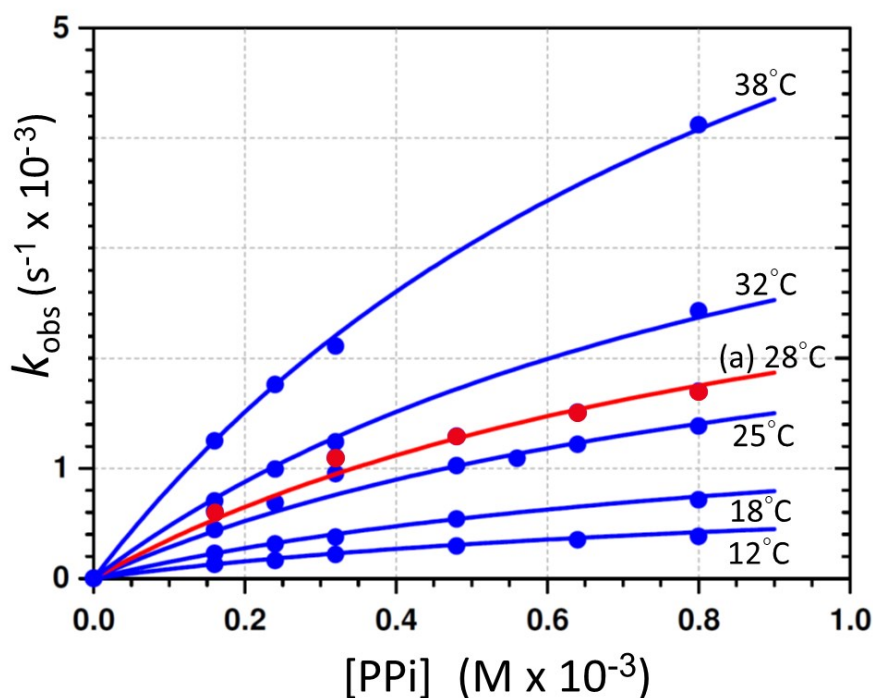
Figure S6: Global L.S. fit of k_{obs} *vs* [PPi]$_{tot}$ at six temperatures: 12, 18, 25, 32, 38°C (Abs vs time) and 28°C (F.I. vs time; (a) red line) and pH 7.35 ([Tris buffer] = 10 mM). The L.S. fit was achieved using Equation 15 above [or Equation (vi), Par. 2]; and the Eyring equation [(Equation (vii), Par. S2] and all the individual k_{obs} values as a function of T and [PPi]$_{tot}$. [Lines indicate L.S. fitted values]

S5. Computational Studies

S5.1. Coordinates and Total Energies of the DFT Optimized Ground-State Structure of [2]
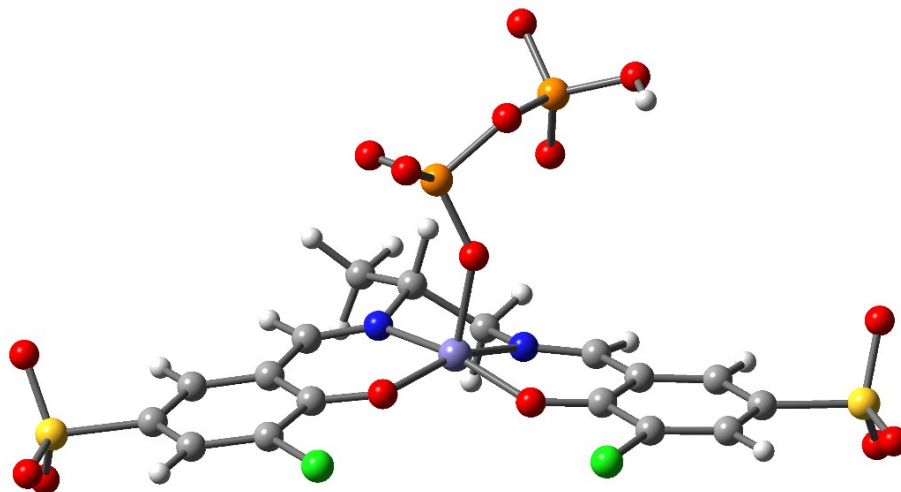
ΔE = 0.0 kcal/mol

Figure S7. A structural representation of DFT Optimized Ground-State Structure of [2].

C	−2.29908900	−1.50510300	0.16240700
C	−3.05630100	−2.50013200	−0.58647300
C	−4.42893800	−2.59686600	−0.45902800
H	−4.99028700	−3.33062400	−1.02577800
C	−5.10590700	−1.74117700	0.41806100
C	−4.40194600	−0.78218900	1.18956100
H	−4.95420300	−0.15768800	1.88389800
C	−3.03160200	−0.64640800	1.07604500
C	−2.35358300	0.30898800	1.92500900
H	−2.97225800	0.82881400	2.65724400
C	−0.48446700	1.48700200	2.87763700
H	−0.16729500	0.88670200	3.73800800
H	−1.21399700	2.22931800	3.20983500
C	0.72601800	2.15671600	2.22425100
H	0.36051400	2.83718400	1.44715000
C	2.71119800	0.94523500	1.46966100
H	3.30762800	1.65144500	2.04341900
C	3.46064100	−0.05677400	0.74058200
C	4.83768400	−0.06137700	0.85304000
H	5.33338100	0.66843800	1.48450900
C	5.62444100	−1.01380000	0.15609200
C	5.02904400	−1.96966500	−0.67431000
H	5.65418900	−2.68419100	−1.19714900
C	3.65410500	−1.99167300	−0.81480100
C	2.80960800	−1.03907600	−0.10591100
N	−1.09074800	0.57003000	1.89195000
N	1.42659600	1.06447600	1.48401300
O	−1.04079300	−1.44255300	−0.00902400
O	1.54927900	−1.11428400	−0.25605000

```
Fe              0.17064400   -0.08692700    0.57625100
O              -0.30387000    1.09006600   -0.88591200
Cl             -2.19640000   -3.53936700   -1.64839800
Cl              2.89174600   -3.15090900   -1.82578200
S              -6.89894800   -1.82067300    0.58395100
O              -7.31938000   -2.99631200   -0.20992400
O              -7.09585300   -1.94538700    2.05150800
S               7.41374900   -0.95708200    0.36465100
O               7.94443800   -2.07391100   -0.44786500
O               7.75352000    0.40228800   -0.13492000
O              -7.32253600   -0.50546200    0.02961800
O               7.57554300   -1.11431400    1.83454000
C               1.57692700    2.93204300    3.22300700
H               2.01557900    2.27510200    3.98118400
H               2.37187500    3.49458700    2.72577200
H               0.93731700    3.65979100    3.73069600
P               0.22836500    2.20707900   -1.79407800
O               1.33256200    3.09450700   -1.21032700
O              -1.11805400    3.11873200   -2.12271400
O               0.79146400    1.78970800   -3.15651900
P              -2.01767900    3.98473900   -1.10801000
O              -1.60624300    5.45835100   -1.02288600
O              -3.46363900    3.85539600   -1.75031800
O              -1.89057300    3.52322400    0.34210100
H              -3.58202200    3.08630700   -2.33772000
```

```
Zero-point correction=                        0.323672 (Hartree/Particle)
Thermal correction to Energy=                          0.364939
Thermal correction to Enthalpy=                        0.365883
Thermal correction to Gibbs Free Energy=               0.241718
Sum of electronic and zero-point Energies=        -5556.199413
Sum of electronic and thermal Energies=           -5556.158147
Sum of electronic and thermal Enthalpies=         -5556.157203
Sum of electronic and thermal Free Energies=      -5556.281368
```

S5.2. Coordinates and Total Energies of the DFT Optimized Ground-State Structure of [3]
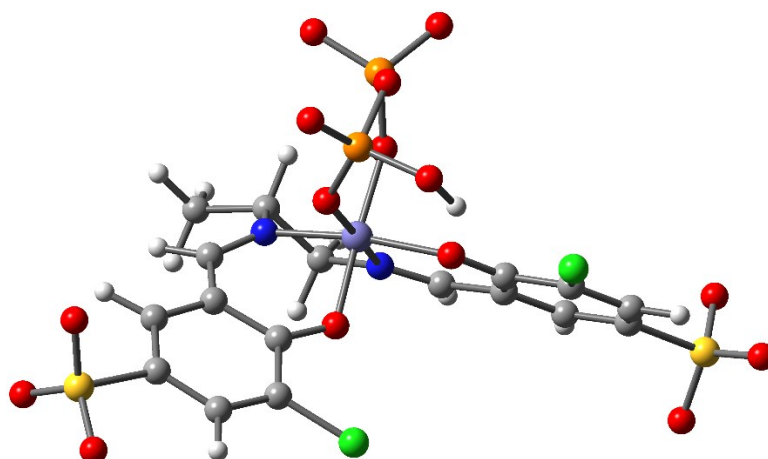
ΔE = -34.1 kcal/mol

Figure S8. A structural representation of DFT Optimized Ground-State Structure of [3].

```
C              2.45080300    -0.39495200     0.35066100
C              3.29675600    -0.96775200     1.39281800
C              4.57267600    -1.41475300     1.11761100
H              5.19463500    -1.83837000     1.89764600
C              5.07228300    -1.32433600    -0.18737500
C              4.28195200    -0.77858500    -1.23032500
H              4.69688900    -0.72342400    -2.23112900
C              2.99864700    -0.32330400    -0.99111600
C              2.25282600     0.21533500    -2.10651700
H              2.78001700     0.24990300    -3.06048900
C              0.40680800     1.20843000    -3.28955100
H             -0.00596100     0.37639700    -3.86989300
H              1.15045900     1.73666200    -3.89041400
C             -0.72620200     2.15560700    -2.85228200
H             -0.29506800     3.04723900    -2.39098900
C             -2.58850400     0.98447800    -1.74635700
H             -3.29157800     1.41838800    -2.45515300
C             -3.05111300    -0.12847200    -0.94438400
C             -4.39552800    -0.41928200    -0.83543900
H             -5.13997700     0.26813300    -1.22231400
C             -4.82051900    -1.63418200    -0.23358700
C             -3.89712800    -2.60096900     0.19073800
H             -4.25851800    -3.52953900     0.61746700
C             -2.54454700    -2.36596400     0.04792400
C             -2.07193900    -1.09358600    -0.48235500
N              1.04072200     0.64962300    -2.07218600
N             -1.36434700     1.38675200    -1.75325400
O              1.27932900     0.00039100     0.65923600
O             -0.81313600    -0.88953900    -0.55635300
Fe            -0.05762900     0.81415800    -0.48625900
O             -1.21696100     1.16738200     0.93287700
Cl             2.66608400    -1.08173900     2.98770700
Cl            -1.38291300    -3.52612800     0.52830300
S              6.73003200    -1.90045300    -0.58487700
O              7.28791900    -2.41933600     0.68190500
O              6.46910600    -2.92684800    -1.62955200
S             -6.58671000    -1.90108100    -0.02725100
O             -6.90509200    -0.86742200     1.00079300
O             -7.14121500    -1.59978700    -1.37062500
O              7.37970500    -0.66731600    -1.10527900
O             -6.73606500    -3.29893600     0.42577400
C             -1.64870500     2.54841700    -3.99778100
H             -2.08946800     1.67670800    -4.49164400
H             -2.44404400     3.21529400    -3.65312500
H             -1.05811100     3.09647800    -4.73745400
P             -1.02067100     1.78582900     2.36327900
O             -2.24717200     2.17068400     3.08761200
O             -0.04566500     3.10006900     2.07647800
O             -0.08184200     0.82583100     3.22810600
P              0.48952800     3.69289200     0.67774700
O              1.78129600     4.47429300     0.91922400
O              0.71978000     2.45326700    -0.26646500
O             -0.45039600     4.74974400     0.09044200
H              0.61641700     0.38425700     2.70533500
```

Zero-point correction=   0.326984 (Hartree/Particle)
Thermal correction to Energy=   0.366380
Thermal correction to Enthalpy=   0.367324
Thermal correction to Gibbs Free Energy=   0.251666
Sum of electronic and zero-point Energies=   -5556.253812
Sum of electronic and thermal Energies=   -5556.214416

```
Sum of electronic and thermal Enthalpies=          -5556.213472
Sum of electronic and thermal Free Energies=       -5556.329130
```

S6.   Evaluation of 1-OH$_2$ Reaction with Monodentate Nucleophile
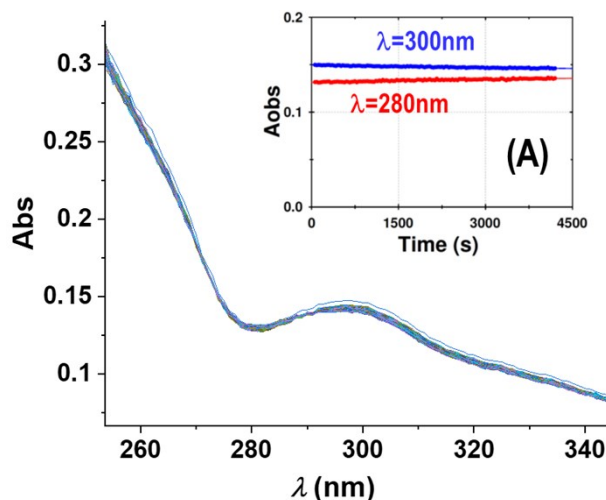
Figure S9. Changes in absorbance of **1-OH$_2$** (16 μM) with time in presence of F$^-$ (10 equiv; 0.16 mM) at pH 7.35 ([Tris buffer] = 10 mM) at 12 ^{o}C. *Inset* (A): Changes in absorbance of **1-OH$_2$** (16 μM) with time at 2 different wavelengths in presence of F$^-$ (10 equiv; 0.16 mM) at pH 7.35 ([Tris buffer] = 10 mM) at 12 ^{o}C and associated *pseudo* first-order fits.
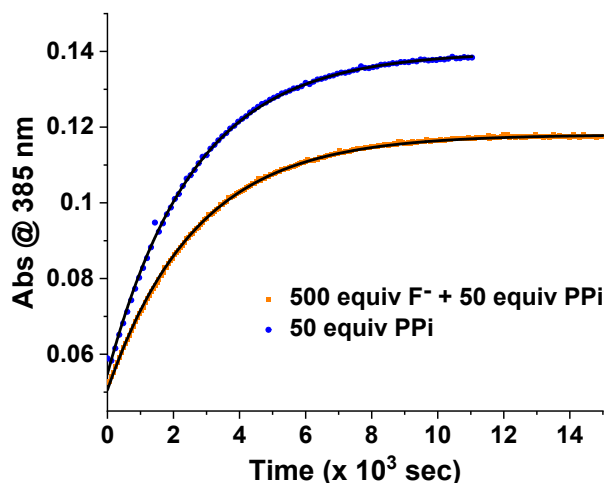
Figure S10. Changes in absorbance at 385 nm of **1-OH$_2$** (16 μM) with time in presence only PPi (50 equiv; 0.80 mM) and both PPi (50 equiv; 0.80 mM) and F$^-$ (500 equiv; 8.00 mM)* at pH 7.35 ([Tris buffer] = 10 mM) at 12 ^{o}C. The respective *pseudo* first-order fitted time traces are also shown; no considerable change in the yielding values of k$_{obs}$ in both cases were found. (k$_{obs\ (F- + PPi)}$ = (0.373 ± 0.001) × 10^{-3} sec; k$_{obs\ (PPi)}$ = (0.383 ± 0.003) × 10^{-3} sec). [Lines indicate

L.S. fits]. *F$^-$ (500 equiv; 8.00 mM) was incubated for almost 10 min before PPi (50 equiv; 0.80 mM) was added.

S7. References

[S1]. P. Yadav, M. Jakubaszek, B. Spingler, B. Goud, G. Gasser, F. Zelder, *Chem. Eur. J.* **2020**, *26*, 5717-5723.

[S2]. R. B. Stockbridge, R. Wolfenden, *J. Biol. Chem*. **2011**, *286*, 18538-18546.